**Showcasing research from Prof. Johannes A. Lercher's group at Technische Universität München.**

Hydrodeoxygenation of fatty acid esters catalyzed by Ni on nano-sized MFI type zeolites

Zeolites with nano-sized crystalline domains provide high mesoporosity while maintaining the microporous structure and well defined acid properties. Here we take advantage of these features for hydrodeoxygenation of algae oil surrogates over supported Ni catalysts. Our results indicate that the nano-sized zeolite allows outstanding Ni dispersion leading to highly active catalysts.
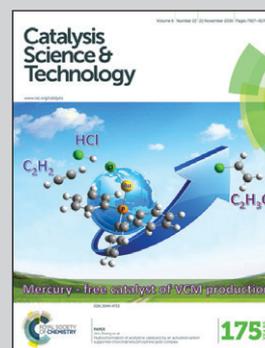
ROYAL SOCIETY OF CHEMISTRY

www.rsc.org/catalysis

Registered charity number: 207890

Hydrodeoxygenation of fatty acid esters catalyzed by Ni on nano-sized MFI type zeolites†

Moritz W. Schreiber,[a] Daniella Rodriguez-Niño,[a] Oliver Y. Gutiérrez*[a] and Johannes A. Lercher*[ab]

The impact of support morphology and composition on the intrinsic activity of Ni supported on MFI-type zeolite was explored in the hydrodeoxygenation of methyl stearate, tristearate, and algae oil (mixture of triglycerides). The nano-sized structure of the support (self-pillared nanosheets) is beneficial for the activity of the catalysts. Higher Ni dispersion and concomitant higher reaction rates were obtained on nano-structured supports than on zeolite with conventional morphology. Rates normalized to accessible Ni atoms (TOF), however, varied little with support morphology. Acidity of the support increases the rate of Ni-catalyzed C–O hydrogenolysis per surface metal site.

Introduction

The conversion of biomass derived oils and fatty acids into transportation fuels is a promising route towards synthesis of renewable energy carriers. Thus, the development of chemical technologies for the conversion of, e.g., mixtures of lipids or phenolic compounds (derived from vegetable/microalgae oils, or pyrolysis oils, respectively), into third generation biofuels has received large interest. Research efforts focus on describing the conversion of complex mixtures of oxygenates to fuel components and on the development of novel stable catalysts.

Active catalysts for the transformation of biomass-derived oils must contain metal and acid functionalities, which lead to efficient deoxygenation through sequences of hydrogenolysis, hydrogenation, and dehydration.[1,2] Deoxygenation of fatty acids proceeds via hydrodeoxygenation (HDO), whereby oxygen is removed by consecutive steps of hydrogenolysis and hydrogenation, or via decarboxylation/decarbonylation (DCO), which does not consume hydrogen but reduces the carbon number of the product. HDO and DCO are typically catalyzed by metals, whereas dehydration readily proceeds on acid sites. The DCO/HDO selectivity on metals, which controls the tradeoff between hydrogen consumption and carbon losses, usually favors HDO over DCO for deoxygenation of fatty acids.[3]

Ni supported on zeolites is one of the most promising systems for deoxygenation, because of its activity, stability and versatility.[2–6] Metal content, particle size of the metal and the acidity of the zeolite can be adjusted using a wide variety of methods.

Whereas the microporosity of zeolites (close to the dimensions of the molecules to be converted) leads to rate enhancement and shape selectivity, it is also associated with potential diffusion limitation and restricted access of substrates to active sites. These problems are more aggravating as the size and complexity of molecules increases.

In order to mitigate the drawbacks of microporosity, while keeping the advantageous structure and well defined acid properties, the crystalline domains have been reduced to nanometric size increasing the fraction of mesopores within the zeolite crystals (hierarchical zeolites).[7,8] Metals supported on such zeolites have been speculated to be more accessible than metals in the pores of conventional zeolites.[9]

To explore this potential advantage, we have prepared Ni catalysts on supports with well-defined zeolite domain sizes and pore systems. That is, MFI type zeolites (silicate and aluminosilicate) with conventional morphology and house of cards organized nanosheets. The Ni loading was kept constant (deposited by deposition–precipitation). The influence of physicochemical properties on the catalytic activity for the deoxygenation of methyl stearate, tristearate, and microalgae oil is explored. A smaller domain size of the zeolite is indeed found to be beneficial for catalytic activity.

Experimental

Synthesis of supports

The aluminosilicate MFI type zeolite with a Si/Al ratio of 90 (H-ZSM-5) was synthesized by adding tetraethyl orthosilicate

[a] Department of Chemistry and Catalysis Research Center, Technische Universität München, Lichtenbergstrasse 4, D-84747 Garching, Germany.
E-mail: Oliver.Gutierrez@mytum.de, Johannes.Lercher@ch.tum.de;
Fax: +0049 89 28913544; Tel: +0049 89 28912827, +0049 89 28913540
[b] Pacific Northwest National Laboratory, Institute for Integrated Catalysis, 902 Battelle Boulevard, Richland, WA 99352, USA

(130 mmol), sodium aluminate (1.44 mmol), and tetra-propylammonium hydroxide (26 mmol) to deionized water (1425 mmol). In the synthesis of silicate MFI type zeolite (Silicalite 1) sodium aluminate was not added to the solution. Aging of the mixtures took place under stirring at room temperature overnight. The aged solutions were transferred into Teflon-lined stainless-steel autoclaves and treated at 443 K for 72 h in a rotating oven with a speed of 30 rpm. After cooling, the resulting suspensions were centrifuged and washed with deionized water. The recovered solids were dried at 343 K overnight and treated in flowing synthetic air (100 ml min^{-1}) at 823 K (heating rate of 2 K min^{-1}) for 8 hours. Subsequently, the powders were stirred in deionized water overnight at 343 K. For the ion exchange, the materials were suspended in 90 mL of 1 M ammonium nitrate solutions and stirred for 5 h at 343 K. The liquid was separated by centrifugation. This step was repeated three times. After drying at 343 K overnight, the materials were finally treated at 823 K (heating rate of 10 K min^{-1}) for 5 h under a flow of synthetic air (100 ml min^{-1}).

Nano-structured self-pillared aluminosilicate zeolite nanosheets with MFI framework (n-H-ZSM-5) and the silicate counterpart (n-Silicalite 1) were prepared according to ref. 8. For the aluminosilicate zeolite material synthesis (Si/Al = 90), tetraethyl orthosilicate (50 mmol) was added dropwise to a 40 vol% solution of tetra-n-butylphosphonium hydroxide (168 mmol) while stirring. To this solution, 9.3 g distilled water and aluminium isopropoxide (1 mmol) was added. The mixture was aged for 12 hours with stirring at room temperature. The solution was transferred to a Teflon-lined stainless steel autoclave and treated for 40 hours at 388 K in a rotating oven at 20 rpm. The product was cooled and washed with distilled water until the pH of the washing solution was lower than 9. The final product was dried for 12 hours at 343 K and treated in flowing synthetic air (100 mL min^{-1}) at 823 K (heating rate of 1 K min^{-1}) for 4 hours.

The synthesis of the self-pillared silicalite nanosheets was performed adding tetraethyl orthosilicate (170 mmol) to a 40 vol% solution of tetra-n-butylphosphonium hydroxide (51 mmol) dropwise while stirring. Distilled water was added and the mixture was stirred for 12 hours at room temperature and transferred to a Teflon-lined stainless steel autoclave and heated for 40 hours at 388 K with stirring. The product was cooled and washed with distilled water until the pH of the washing solution was lower than 9. The final product was dried for 12 hours at 343 K and treated in flowing air (100 mL min^{-1}) at 823 K (heating rate of 1 K min^{-1}) for 12 hours. The materials were stirred in a suspension of distilled water for 12 h at 343 K. The proton forms of the materials were obtained by mixing the solids with 1 M solutions of ammonium nitrate. This suspension was heated at 343 K while stirring for 5 hours and the solid was recovered by centrifugation. This process was repeated three times. The final product was dried at 343 K for 12 hours and treated in flowing synthetic air (100 mL min^{-1}) at 673 K (heating rate of 1 K min^{-1}) for 4 hours.

Synthesis of Ni catalysts

Ni was incorporated *via* the deposition–precipitation method.[10] The procedure consisted in preparing a solution of nickel nitrate (35 mmol) in 250 mL of deionized water. An aliquot of 40 mL of this solution was used for dissolving urea (105 mmol) and the remaining volume (210 ml) was mixed with a sample of solid support. The suspension was refluxed at 363 K. When the temperature of the suspension reached 343 K, the solution of nickel nitrate and urea was added dropwise. After 43 min at 363 K, the suspension was cooled to room temperature, filtered and the solid was washed with deionized water at 333 K. After drying at 343 K for 24 h, the catalyst precursor was subsequently treated in flowing synthetic air (100 mL min^{-1}) at 673 K (heating rate of 1 K min^{-1}) for 4 h and in H$_2$ (100 mL min^{-1}) at 733 K (heating rate of 2 K min^{-1}) for 4 h.

Chemical and physicochemical characterization

Elemental analysis of all materials was performed *via* atomic adsorption spectroscopy with an Unicam M Series Flame-AAS instrument equipped with an FS 95 auto-sampler and a GF 95 graphite furnace. Powder X-ray diffraction patterns were recorded with a Philips X'Pert Pro system (λCuK$_\alpha$ = 0.154056 nm, 40 kV/40 mA) with a step size of 0.017° and a scan speed of 0.3 s per step. Transmission electron micrographs were recorded with a JEOL JEM-2011 TEM instrument with a maximum acceleration of 120 kV. Scanning electron microscopy measurements were performed on a JEOL JSM 7500F SEM. Shape, primary particle size and morphology of the materials were determined from TEM and SEM images. Particle size determination was done based on the evaluation of at least 300 particles. Nitrogen physisorption was carried out at 77 K on a PMI automated sorptometer after outgassing the samples under vacuum at 523 K for 2 h. The BET isotherm was used to evaluate the apparent specific surface area over a relative pressure range of 0.01–0.1 p/p_0. The micro- and mesopore volumes were evaluated by using non-porous hydroxylated silica as the reference adsorbent.[11] The macro-pore volume was calculated by subtracting micro- and mesopore volumes from the total pore volume determined at p/p_0 = 0.95. The pore size distribution of the zeolites was evaluated by the DFT method (cylindrical pore, NLDFT equilibrium model).

The concentration of chemisorbed H$_2$ on Ni was determined with a Sorptomatic 1990 instrument. Samples were treated in a flow of H$_2$ at 723 K for 1 h and then evacuated at the same temperature for 1 h before measurements. Hydrogen adsorption was conducted at 307 K in a pressure range of 0.5–13.2 kPa with an equilibration time of 5 min. After completing the first isotherm, the sample was evacuated to 10^{-4} kPa and a second isotherm was measured. The second isotherm (physisorption) was subtracted from the first one. The amount of chemisorbed hydrogen was determined by extrapolating the linear part of the difference isotherm ($P > 6.5$ kPa) to zero pressure. The concentrations of chemisorbed H$_2$ were calculated assuming an H/Ni stoichiometry of 1.

This journal is © The Royal Society of Chemistry 2016

Catal. Sci. Technol., 2016, **6**, 7976–7984 | 7977

Infrared spectroscopy of adsorbed pyridine and 2,6-di-*tert*-butyl-pyridine (2,6-DTBPy) as probe molecules was used to determine the total concentration and location of Brønsted and Lewis acid sites.[12,13] The instrument used for the experiments was a Thermo Nicolet 5700 FT-IR spectrometer with a resolution of 4 cm^{-1}. All samples were pressed into self-supporting wafers (density ~0.01 g cm^{-1}) and activated under vacuum ($p < 10^{-7}$ kPa) for 1 h at 723 K (heating rate of 10 K min^{-1}). The activated materials were exposed to pyridine or 2,6-DTBPy at 0.01 kPa and 423 K for 0.5 h and evacuated for 1 h to desorb weakly bound molecules. The bands at ~1545 cm^{-1} and ~1450 cm^{-1} were integrated to determine the total concentration of Brønsted and Lewis acid sites, respectively. The samples were subsequently heated to 723 K (10 K min^{-1}) for 0.5 h in vacuum to determine the concentration of strong Brønsted and Lewis acid sites. The concentration of Brønsted acid sites interacting with 2,6-DTBPy was calculated by integrating the N–H$^+$ stretching vibration band at 3367 cm^{-1}.[13] All spectra were collected at 423 K. The acid site concentrations reported were normalized to the weight of the sample.

Activity tests

The experiments were performed in a 45890HP Parr vessel. Preliminary experiments employing varying particle sizes and stirring rates discarded the presence of diffusion artefacts. All reactions were conducted at a H$_2$ pressure of 40 bar with 84.7 mg (5 mmol) of eicosane as an internal standard and 45 g of dodecane as solvent. 89.5 mg (5 mM) methyl stearate, or tristearate (1.66 mM), or 89.5 mg microalgae oil (the composition of microalgae oil is given in Table S1†) were used as reactants. Samples of 30 mg of the catalysts were reduced as described before and immediately employed in the reaction. Catalyst stability was tested using Ni/n-H-ZSM-5 in the conversion of microalgae oil in four consecutive runs. After each run, new reactant solution was introduced into the reactor. This was performed under H$_2$ flow in order to avoid exposure of the catalyst to air. Prior to the reaction, the reactor was filled with 15 bar H$_2$ and purged three times. As soon as the temperature reached 553 K, the pressure inside the reactor was set to 40 bar with H$_2$. Aliquots of the liquid phase were periodically extracted from the reactor and analyzed offline by a gas chromatograph (GC, Agilent Technologies 7890B GC) connected to a flame ionization detector (FID) and a mass spectrometer (MS, Agilent Technologies 5977A). The GC was equipped with a HP-5 capillary column. Quantification was done based on the internal standard and an external calibration of the GC-FID signal of each compound. The molar carbon balance was always higher than 97%. The gas phase was analyzed offline with an Agilent 7890B gas chromatograph with a FID. The GC was equipped with molsieve 13x, DB-1, and Hayesep Q columns.

Reaction orders of methyl stearate and triglyceride conversions were determined to be unity using the integrated rate law. First-order rate constants were calculated taking into account the complete concentration profiles. The R^2 value of the regression line was typically above 0.98.

Results and discussion

Characterization

Four parent supports and four Ni catalysts were obtained by the procedures described above. In the following the supports are labeled as H-ZSM-5 (aluminosilicate MFI type zeolite with conventional porosity), Silicalite 1 (silicate MFI type zeolite with conventional porosity), n-H-ZSM-5 (aluminosilicate zeolite with MFI framework and self-pillared nanosheet structure), and n-Silicalite 1 (silicate zeolite with MFI framework and self-pillared nanosheet structure). The corresponding catalysts are denoted as Ni/H-ZSM-5, Ni/Silicalite 1, Ni/n-H-ZSM-5, and Ni/n-Silicalite 1.

Characterization of the catalysts

Representative TEM images of the catalysts are shown in Fig. 1. In the materials with conventional morphology (Ni/H-ZSM-5 and Ni/Silicalite 1), the particles of the support have projected rectangular shapes of about 200 × 360 nm. SEM images (Fig. S1 in the ESI†) of the support confirmed this shape. The small agglomerates observed at the perimeters of the supports in TEM images are identified as Ni particles. In contrast, the supports with nano-sized structure (Ni/n-H-ZSM-5 and Ni/n-Silicalite 1) consist of round rough particles with diameters of about 100 nm. These particles are agglomerates of orthogonally linked microporous nanosheets with height of 8 nm and lengths of 20–100 nm. The Ni particles are observed as small dark dots within the crystalline domains and on the outer surface of the support particle. The morphologies of H-ZSM-5 and Silicalite 1 were nearly identical within the conventional or nano-structured series. The morphologies shown in Fig. 1 for the nano-structured materials (Ni/n-H-ZSM-5) allow to assign the broad distribution of mesopores detected by N$_2$-physisorption (*vide infra*) to cavities between the nano-sized crystals and to inter-crystalline voids between the particles. Moreover, the Ni particles observed in Fig. 1 evidence the large differences of Ni particle sizes between the series with conventional and nano-structured morphology.

The X-ray patterns of the catalysts (Fig. S2 and S3 in ESI†) show the characteristic main reflections at 2θ = 8.3°, 9.2°, 23.5°, 24.3°, and 24.8° of MFI framework zeolites.[14] The patterns of the nanosheet materials (Ni/n-H-ZSM-5 and Ni/n-Silicalite 1) have peaks at the same positions although broader. This indicates that the same crystallographic phase is present in all materials although with very different crystal size. The broader XRD reflections of the n-H-ZSM-5 materials are caused by the small crystalline domains.[8] The X-ray diffractograms of the parent supports show also that the MFI framework was not affected by the Ni deposition. The X-ray diffractograms of the catalysts showed, moreover, reflections at 2θ = 44.5°, and 52.8°, assigned to the (111) and (200) planes of Ni (FCC).

7978 | *Catal. Sci. Technol.*, 2016, **6**, 7976–7984

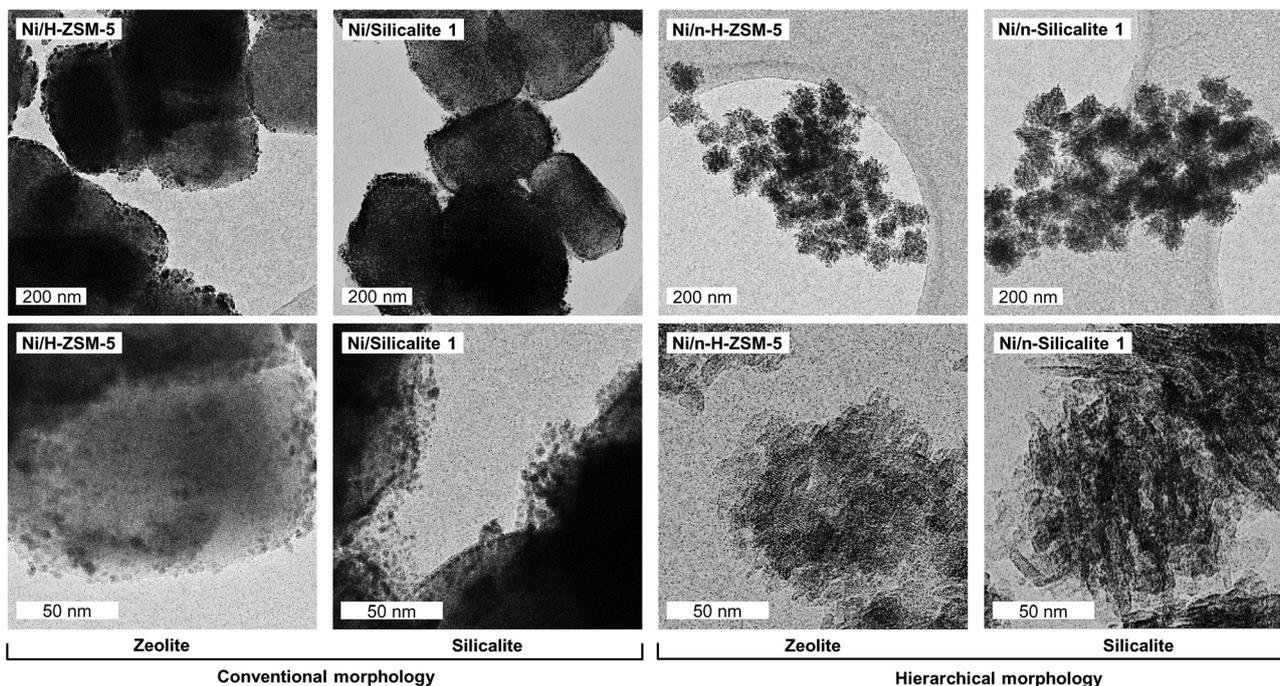This journal is © The Royal Society of Chemistry 2016

Fig. 1 Representative micrographs of Ni supported on (n)-H-ZSM-5 and (n)-Silicalite 1 materials. Note the cross-linking between crystalline sheets for the nanosheet materials (n-H-ZSM-5 and n-Silicalite 1), which produces mesoporosity. The dark dots in all images are nickel particles.

The micropore and mesopore volumes (V_{micro}, and V_{meso}, respectively) of the catalysts with conventional and nano-structured structure differed greatly (Table 1). The nanosheet materials (Ni/n-H-ZSM-5 and Ni/n-Silicalite 1) had mesopore volumes, which were one order of magnitude higher than those of conventional counterparts (Ni/H-ZSM-5 and Ni/ Silicalite 1). The micropore volumes of the nanosheet materials were, in contrast, 2.5 times smaller than those of the materials with conventional morphology. Deposition of Ni led to a decrease of the micropore volume of nanosheet materials by a factor of 10 (Table 1). This indicates that Ni particles either selectively fill or block a large fraction of micropores of the nano-structured materials. The Si/Al molar ratios of the aluminosilicate materials were comparable (92 and 108 for H-ZSM-5 and n-H-ZSM-5, respectively).

The N_2 physisorption isotherms and pore size distributions of the materials hardly changed upon Ni deposition

(Fig. 2, and Fig. S5†). The series of materials with conventional morphology shows type I isotherms, typical for microporous materials, whereas the series with nano-structured morphology exhibits type IV isotherms with hysteresis loops at relative pressures above 0.6, indicative of mesoporous systems. Fig. 2 shows the homogeneous distribution of micropores in the series with conventional morphology and the large contribution of mesopores (with diameters mainly below 150 Å) for the series with nano-structured morphology.

Quantification of the acid sites at the external surface of the zeolite was performed via adsorption of 2,6-di-tert-butyl-pyridine (2,6-DTBPy). The difference spectrum, i.e., the spectrum of the zeolite subtracted from the spectrum recorded after 2,6-DTBPy adsorption (Fig. S4 in ESI†) showed that a fraction of terminal SiOH groups (3745 cm^{-1}) and Brønsted acid sites (3610 cm^{-1}) interacted with 2,6-DTBPy, as the intensity of both bands decreased. New bands appeared at 3370 cm^{-1}

Table 1 Ni content (Ni), accessible Ni atoms (accessible Ni), Si/Al molar ratio (Si/Al), total pore volume (V_{total}), micropore volume (V_{micro}), mesopore volume (V_{meso}), average mesopore diameter ($Ø_M$), and Ni particle diameter ($Ø_{Ni}$) of supports and catalysts

Material	Ni [wt%]	$Ø_{Ni}^{a}$ [nm]	Accessible Ni^{a} [μmol g^{-1}]	Si/Al	V_{total} [cm^3 g^{-1}]	V_{micro} [cm^3 g^{-1}]	V_{meso} [cm^3 g^{-1}]	$Ø_M$ [nm]
H-ZSM-5	—	—		92	0.21	0.14	0.07	—
Silicalite 1	—	—		—	0.18	0.13	0.09	—
n-H-ZSM-5	—	—		108	0.95	0.055	0.90	20
n-Silicalite 1	—	—		—	0.84	0.06	0.78	20
Ni/H-ZSM-5	9.7	12.9	128	92	0.22	0.15	0.07	—
Ni/Silicalite 1	10.1	8.4	207	—	0.24	0.13	0.11	—
Ni/n-H-ZSM-5	9.3	4.5	349	108	0.80	0.004	0.79	20
Ni/n-Silicalite 1	9.8	4.7	370	—	0.76	0.006	0.75	20

^{a} Determined based on H_2 chemisorption and elemental analysis.

This journal is © The Royal Society of Chemistry 2016

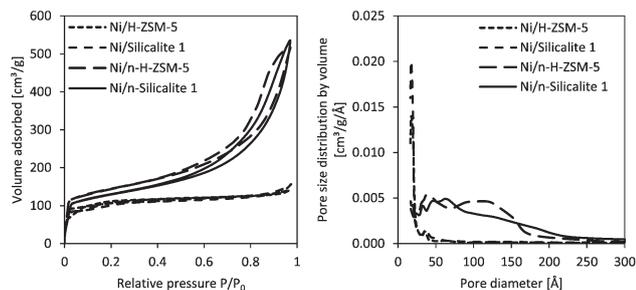Catal. Sci. Technol., 2016, 6, 7976–7984 | **7979**

Fig. 2 N$_2$-Physisorption isotherms and pore size distributions of Ni catalysts.

and 1616 cm^{-1}, which are assigned to the N–H$^+$ vibration of protonated 2,6-DTBPy and to one of its C=C ring vibrations, respectively.[13]

The acidities of the zeolites, as determined by IR spectroscopy of adsorbed pyridine and 2,6-DTBPy are summarized in Table 2. The total concentration of acid sites was comparable for both materials, i.e., 45–52 µmol g^{-1} Lewis acid sites, and 153–173 µmol g^{-1} Brønsted acid sites for H-ZSM-5, and n-H-ZSM-5, respectively. However, most of the acid sites on n-H-ZSM-5 were strong, whereas 50% of LAS and 33% of BAS in H-ZSM-5 were weak. Comparisons of the adsorption of pyridine and 2,6-DTBPy indicated that only 10% of BAS (17 µmol g^{-1}) were accessible for 2,6-DTBPy in H-ZSM-5, whereas 43% of the BAS (66 µmol g^{-1}) were accessible in n-H-ZSM-5.

The Ni catalysts contained Ni loadings of around 10 wt%. The dispersion of the metal was assessed by XRD, TEM and H$_2$ chemisorption (Table S2 of the ESI†). Although there are variations for the dispersions of small Ni particles, the trends are identical within the results derived from a specific technique. The average particle sizes of Ni particles were smaller on nanosheet materials than on materials with conventional morphology, whereas Ni particles have very similar sizes within the series (d (Ni/H-ZSM-5) ≈ d (Ni/Silicalite 1) < d (Ni/n-H-ZSM-5) ≈ d (Ni/n-Silicalite 1)). Small metal particles may escape from detection in XRD and TEM measurements. The former technique is limited to particles with crystalline domains large enough to produce coherent reflection, while the latter is limited by the resolution of the instrument and size of the metal particles. H$_2$ chemisorption, in contrast, titrates the surface atoms of the metal particles independently of their size. Therefore, the results obtained by H$_2$ chemisorp-

tion (Table 1) were used for calculation of intrinsic activities. The concentrations of accessible Ni atoms varied by a factor of 3 between H-ZSM-5 and n-H-ZSM-5, i.e., 128 µmol g^{-1} and 349 µmol g^{-1}, respectively.

Catalytic activity and selectivity

Catalytic activity and selectivity of Ni catalysts (pure (n)-H-ZSM-5 or (n)-Silicalite 1 are not active) for HDO of methyl stearate, tristearate, and microalgae oil were investigated. The kinetic results are compiled in Fig. 3, 4, and S4,† and in Tables 3 and 4.

Hydrodeoxygenation of methyl stearate

The specific activity (per mass of catalyst) increased in the case of Ni on aluminosilicates and was always higher for the hierarchic material, i.e., Ni/Silicalite 1 < Ni/n-Silicalite 1 < Ni/H-ZSM-5 < Ni/n-H-ZSM-5 (Table 3). Thus, the mesoporosity improved the reaction rates twofold (e.g., k = 0.36 h^{-1} on Ni/Silicalite 1, compared to k = 0.75 h^{-1} on Ni/n-Silicalite 1), while the use of aluminosilicate instead of silicate based zeolites enhanced the rate by a factor of 3 (e.g., k = 0.36 h^{-1} on Ni/Silicalite 1, compared to k = 1.16 h^{-1} on Ni/H-ZSM-5). The rate of conversion on Ni/n-H-ZSM-5 was faster than on Ni/H-ZSM-5 by a factor of 4. The activity of Ni supported on nano-structured zeolite (Ni/n-H-ZSM-5), however, was one order of magnitude higher than Ni supported on microporous silicate (Ni/Silicalite 1). That is, the combination of using a zeolite and mesoporosity had a synergistic effect on the activity of the supported metal.

The analysis of the intrinsic activity shows a different picture. The variation of TOFs follows the same trend as that of specific rates (Ni/Silicalite 1 ≤ Ni/n-Silicalite 1 ≪ Ni/H-ZSM-5 ≤ Ni/n-H-ZSM-5). Within the experimental error (±10%), however, TOF on the silicalite based catalysts (Ni/Silicalite 1 and Ni/n-Silicalite 1) are the same (∼20 h^{-1}), whereas for the zeolite based catalysts the activity of Ni/n-H-ZSM-5 is higher than that of Ni/H-ZSM-5 only by 30%. In a word, a nano-structured pore system has little effect on the activity of Ni supported on silicalite and a modest one on the activity of Ni on zeolites. Supporting the Ni particles on aluminosilicate zeolites (H-ZSM-5 or n-H-ZSM-5), on the other hand, increases the intrinsic activity of Ni by a factor of ∼5 compared to supporting

Table 2 Concentrations of acid sites of the conventional and the nano-structured materials

Material	Total acid sites[a] [µmol g^{-1}]		Strong acid sites[b] [µmol g^{-1}]		Weak acid sites[c] [µmol g^{-1}]		Accessible BAS[d] [µmol g^{-1}]	Inaccessible BAS[e] [µmol g^{-1}]
	LAS	BAS	LAS	BAS	LAS	BAS		
H-ZSM-5	46	173	24	115	22	58	17	156
n-H-ZSM-5	52	153	50	152	1	1	66	87

[a] After adsorption of pyridine at 423 K and outgassing for 1 h under vacuum. [b] After subsequently heating the samples of [a] to 723 K for 0.5 h under vacuum. [c] Difference between total concentration of Brønsted/Lewis acid sites and concentration of strong Brønsted/Lewis acid sites. [d] Calculated based on the percentage of 2,6-DTBPy interacting with total Brønsted acid sites. [e] Difference between total concentration of Brønsted acid sites (both strong and weak) and concentration of Brønsted acid sites accessible for 2,6-DTBPy.
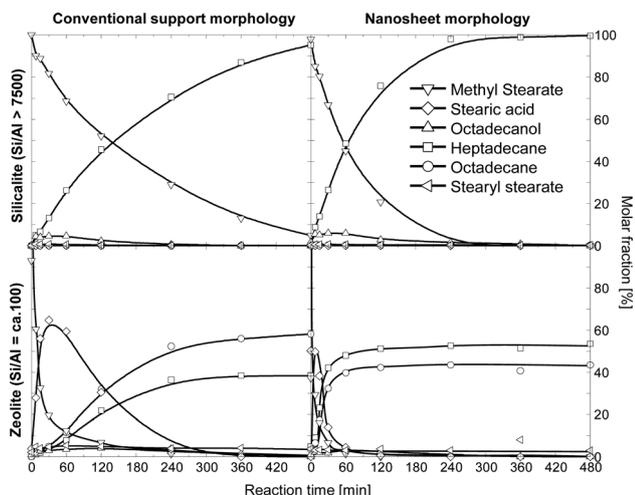
Fig. 3 Evolution of the concentrations of methyl stearate and reaction products over time on the catalysts with different morphology and acidity. Reaction carried out with methyl stearate as reactant (5 mmolar in dodecane) at 40 bar H_2 and 553 K.
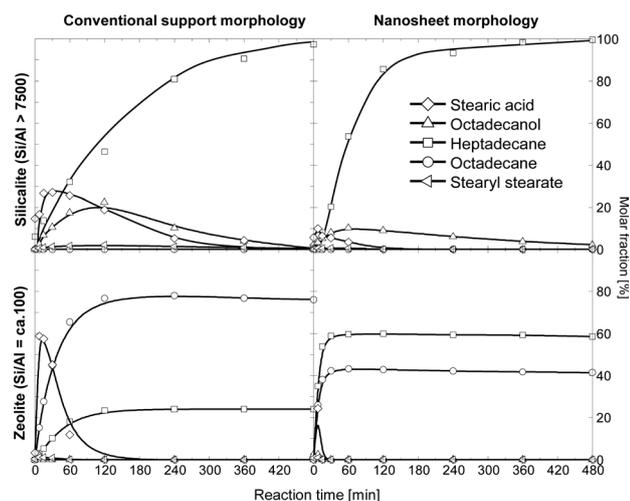

Fig. 4 Evolution of the concentrations of reaction products of tristearate conversion over time on the catalysts with different morphology and acidity. Reaction carried out with tristearate as reactant (1.66 mmolar in dodecane) at 40 bar H_2 and 553 K.

the metal on the corresponding silicate zeolites (Silicalite 1 or n-Silicalite 1).

Fig. 3 shows the evolution over time of the concentration of methyl stearate and the products. Stearic acid, stearyl

stearate, and octadecanol are intermediate products, having concentrations that pass through maxima; whereas octadecane and heptadecane are final products. These observations allow us to propose the reaction network shown in Fig. 5 in agreement with previous reports.[4] Stearic acid is produced by a hydrogenolytic C–O cleavage of methyl stearate or triglyceride, which produces methane or propane as by-products (only alkanes were detected in the gas phase). Hydrolysis of methyl stearate to methanol and stearic acid was excluded, as methanol was not detected in the gas and liquid phases while conversion over pure zeolite (which could have catalyzed hydrolysis *via* Brønsted acid sites) was not observed. A second hydrogenolysis step converts the acid to the highly reactive aldehyde intermediate (stearic aldehyde, not observed in this work), which undergoes decarbonylation to heptadecane, or hydrogenation to octadecanol. Direct decarboxylation of stearic acid, observed over Pt and Pd,[3] is excluded on Ni catalysts because stearic acid was not converted under N_2 atmosphere. Dehydration of octadecanol (yielding octadecene), and consecutive hydrogenation leads to octadecane as a final product. In parallel to the described steps, esterification of stearic acid and octadecanol yields stearyl stearate only on aluminosilicate-based catalysts (Ni/H-ZSM-5 and Ni/n-H-ZSM-5), when stearic acid is present in relatively high concentrations.

Stearic acid was not observed on silicate based catalysts (Ni/Silicalite 1 and Ni/n-Silicalite 1), which implies that the hydrogenolysis of the Csp^2–O bond of the acid is faster than that of the Csp^3–O bond of the methyl stearate. Furthermore, octadecane is not observed and very low concentrations of octadecanol are formed. This is due to the absence of Brønsted acid sites, which hinders the dehydration of octadecanol. As a consequence, only the decarbonylation pathway towards heptadecane is available to convert the octadecanal–octadecanol pair, which likely reaches equilibrium even at low reaction times.

In contrast to Ni supported on silicates, stearic acid was observed on aluminosilicate based zeolites (Ni/H-ZSM-5 and Ni/n-H-ZSM-5), which indicates that the Csp^3–O hydrogenolysis of the methyl stearate is faster than that of the Csp^2–O bond of the fatty acid. As the aluminosilicate catalysts are much more active than the silicalite counterparts, we conclude that supporting Ni on zeolite enhances the Csp^3–O cleavage to a larger extent than the Csp^2–O cleavage. The most distinctive feature of Ni on aluminosilicate zeolites

Table 3 First order reaction rate constant, initial rate and turn-over frequency for the hydrodeoxygenation of methyl stearate

Catalyst	Reaction rate constant k^a [h^{-1}]	Initial reaction rate r_0^b [mmol (h g_{cat})$^{-1}$]	Turnover frequency^c [$mol_{reactant}$ ($mol_{accesible\ Ni}$ h)$^{-1}$]
Ni/H-ZSM-5	1.16	12.0	94
Ni/Silicalite 1	0.36	4.0	19
Ni/n-H-ZSM-5	4.42	44.0	126
Ni/n-Silicalite 1	0.75	8.0	22

^{a} Calculated *via* the integrated rate law taking into account the concentration profile during the entire reaction time. ^{b} Calculated at zero reaction time as the product of the rate constant and initial concentration. ^{c} Determined by normalizing the initial rates with the concentration of surface Ni atoms.

This journal is © The Royal Society of Chemistry 2016

Catal. Sci. Technol., 2016, **6**, 7976–7984 | 7981

Table 4 First order reaction rate constant, initial rate and turn-over frequency for the hydrodeoxygenation of tristearate, and microalgae oil[a]

Catalyst	Reaction rate constant[b] [h^{-1}]		Initial reaction rate r_0[c] [mmol (h g_{cat})$^{-1}$]		Turnover frequency[d] [$mol_{reactant}$ ($mol_{accesible\ Ni}$ h)$^{-1}$]	
	Tristearate	Microalgae oil	Tristearate	Microalgae oil	Tristearate	Microalgae oil
Ni/H-ZSM-5	2.0	2.6	20.2	25.8	158	201
Ni/Silicalite 1	0.4	0.3	3.5	3.1	17	15
Ni/n-H-ZSM-5	8.4	8.0	84.0	80.4	241	230
Ni/n-Silicalite 1	1.1	0.9	10.7	8.9	29	24

[a] The parameters corresponding to tristearate and microalgae oil were calculated based on the product formation with first order kinetics. [b] Calculated by dependence of conversion on reaction time with first order kinetics. [c] Calculated at zero reaction time. [d] Determined by normalizing the initial rates with the concentration of surface Ni atoms (ESI).

is that octadecane is the main final product, which indicates that the dehydration of octadecanol, followed by hydrogenation of the octadecene intermediate is faster than the decarbonylation of octadecanal.

Hydrodeoxygenation of tristearate and microalgae oil

While the sequence of catalytic activities for tristearate and microalgae oil, normalized to mass of catalyst, was the same than that observed for methyl stearate, i.e., Ni/Silicalite 1 < Ni/n-Silicalite 1 < Ni/H-ZSM-5 < Ni/n-H-ZSM-5 (Table 4), it should be noted that the reactivity of methyl stearate was lower than that of tristearate or microalgae oil. We hypothesize that this is caused by a higher heat of adsorption of the latter, directly influencing the measured rates, as the reaction order was determined to be one. Considering the performance of Ni/Silicalite 1 as the reference, catalysts with nanostructured supports were approximately three times more active. Similar observations were made for the conversion of microalgae oil. The use of zeolite instead of silicalite as a support enhanced the rate by a factor of five (e.g., k = 0.4 h^{-1} on Ni/Silicalite 1, compared to k = 2 h^{-1} on Ni/H-ZSM-5). The

conversion rates on Ni/n-H-ZSM-5 were higher than on Ni/H-ZSM-5, and Ni/Silicalite 1 by factors of 4 and 20, respectively. Thus, the use of zeolite and hierarchical pore systems have positive effects on the activity of the catalysts for the conversion of the three feeds.

Despite of different morphologies (conventional or nano-structured), TOFs are comparable on materials with the same composition (aluminosilicate or silicate) following the trend Ni/Silicalite 1 ≤ Ni/n-Silicalite 1 ≪ Ni/H-ZSM-5 ≤ Ni/n-H-ZSM-5. Thus, the hierarchic materials stabilize smaller Ni particles and the higher reaction rates per mass of catalyst on Ni supported on nano-structured materials are due to better metal dispersion. In contrast, the use of zeolite instead of silicalite as a support enhances the TOF by an order of magnitude (e.g., TOF = 17 h^{-1} on Ni/Silicalite 1, compared to 158 h^{-1} on Ni/H-ZSM-5).

The products of tristearate conversion in the liquid phase were identical to the products observed for methyl stearate conversion, i.e., stearic acid, stearyl stearate, octadecanol, octadecane and heptadecane. This indicates direct Csp^3–O hydrogenolysis of the ester bond of glycerol and stearic acid. The product distributions, including the evolution of products over time, for the HDO of tristearate and microalgae oil are similar (Fig. 4 and Fig. S6†). On the catalysts based on aluminosilicate zeolite with conventional morphology, the conversion of triglyceride yielded more octadecane than the conversion of methyl stearate. We attribute this to competitive adsorption of methyl stearate on Brønsted acid sites, which reduces the rate of octadecanol conversion to octadecane. In contrast, the triglycerides are too bulky to access the micropore system of the zeolite, where most of the acid sites are located. Thus, dehydration of the alcohol on Brønsted acid sites occurs rapidly in the presence of triglycerides, resulting in higher selectivity to octadecane than in the presence of methyl stearate. Besides this, the evolution of reactant and products and their dependence on catalyst composition is the same as that described for methyl stearate. Thus, the nature of the reactants (methyl stearate, tristearate, or a mixture of triglyceride) mainly influences the overall rates, whereas the selectivities are affected to a lower extent. A general reaction network is shown in Fig. 5.

During recycling experiments, the reaction rate of triglyceride conversion on Ni/n-H-ZSM-5 stayed constant within the
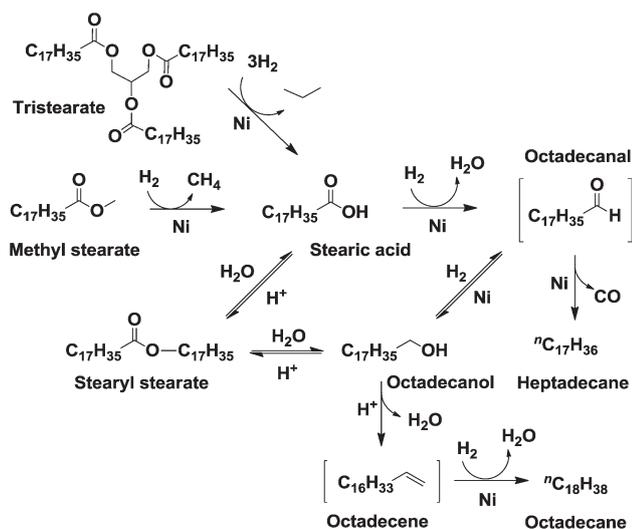

Fig. 5 Reaction network for the hydrodeoxygenation of tristearate and methyl stearate. "Ni" and "H⁺" denote steps catalyzed by metal or Brønsted acid sites. Compounds in brackets were not observed in this study.

7982 | *Catal. Sci. Technol.*, 2016, **6**, 7976–7984

This journal is © The Royal Society of Chemistry 2016

measuring error (Fig. S7†). Changes in the reaction order were not detected, *i.e.*, a first order behavior was observed in all runs. Hence, deactivation does not take place under the reaction conditions explored. In line with the catalytic stability, the X-ray diffractograms of the spent catalysts were almost identical to those of the fresh catalysts (Fig. S8 and S9†). This indicates that the support and Ni particles are structurally stable under the conditions applied in this study.

On the effects of mesoporosity and composition of the support on the hydrodeoxygenation reactions

Nickel catalyzes the initial hydrogenolytic steps of the reaction network. The Brønsted acid sites, on the other hand, catalyze the conversion of the intermediately formed alcohol *via* dehydration or esterification. This is an important role, because the selectivity of the final products depends to a large extent on the ability of the catalyst to dehydrate the alcohol. If this functionality is missing, carbon loss *via* decarbonylation on Ni is favored.[15]

The question arises as to how the presence of mesoporosity influences the performance of the catalysts. The results here demonstrate that nano-structured systems lead to more active catalysts than large crystal MFI type zeolites in line with results obtained for catalysts supported on BEA.[16] The main cause for the higher activities is the higher dispersion of Ni of the nano-structured materials. Note that the concentration of exposed Ni atoms is up to a factor of 3 higher on the nanostructured materials than on the typical morphologies. This is likely due to the high specific surface area accessible to deposit Ni particles in the nano-structured supports compared to the conventional counterparts.

The morphology of the support showed only a modest positive effect on the intrinsic metal activity *i.e.*, the ratios of the TOFs observed on nano-structured catalysts divided by the TOFs observed on conventional catalysts are all above 1 but below 2. Therefore, there are not large differences in the concentration of Ni sites available for methyl stearate, tristearate, and triglycerides on the catalysts. Consequently, as the examined triglycerides are too bulky to enter the micropore system of MFI type zeolites, the majority of the active Ni has to be located on the outer surface of the supports.

The dimensions of support and nickel particles in different catalysts as well as the triglyceride are schematically compared in Fig. 6. The figure shows the higher Ni dispersion on the nano-structured materials.

The main factor increasing the intrinsic activity of the catalyst is the composition of the support. We attribute this promoter effect to acidity as it is the only property intrinsically changing with composition. This metal-support effect is known for hydrogenation,[17,18,25] C–C hydrogenolysis,[19,25] ring enlargement,[20,25] and isomerization.[21,25] Effects of acid sites on C–O cleavage, however, have been reported only recently.[22–24] Many explanations have been put forward for this effect, *e.g.*, decreased electron density at the metal due
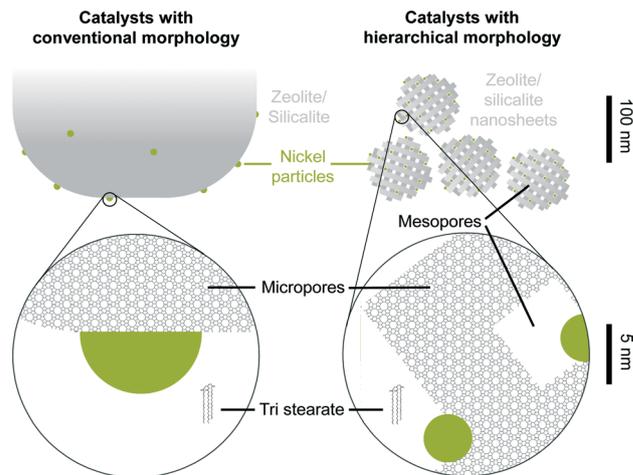

Fig. 6 Graphical representation of catalysts with conventional and nano-structured morphology.

to withdrawing toward acid sites,[19] and interactions of metal sites and protons of the BAS.[26] All theories invoke increasing polarization of the metal sites. Our results suggest that this polarization originates from a direct interaction between Brønsted acid sites with Ni particles, as a significant Brønsted acid site concentration was found on the outer surface/pore mouths of both aluminosilicate based catalysts. However, it is not in the scope of this work to test this proposal. Further studies are being carried out.

Conclusions

Ni catalysts supported on hierarchical materials, *i.e.*, self-pillared nanosheets, are more active in deoxygenation of methyl stearate, tristearate, and algae oil than the counterparts with conventional structure. The high Ni activity attained on the hierarchical materials are due to outstanding metal dispersion as rates normalized to accessible Ni (TOF) on catalysts with hierarchical and conventional structure are comparable. TOFs of methyl stearate and triglyceride conversion, being independent of support morphology, indicate that the majority of Ni particles are located on the outer surface of the supports (triglycerides are too bulky to access the micropore system of MFI type zeolites).

Interestingly, the acidity of the support has a strong positive influence on the intrinsic activity of Ni. Therefore, the most active catalyst relies on the highest Ni dispersion in the presence of nano-sized crystallites as well as on the highest concentration of acid sites.

Overall, self-pillared zeolite nanosheets have an important potential as catalytic supports for bulky reactants that do not access the microporous system. This is because its small particle sizes and hierarchical support morphology increase the concentration of accessible acid sites by factors of 3–4 and provide a one order of magnitude higher mesopore volume for metal deposition compared to conventional zeolite supports.

This journal is © The Royal Society of Chemistry 2016

Catal. Sci. Technol., 2016, **6**, 7976–7984 | 7983

Acknowledgements

References

1 J. C. Serrano-Ruiz, R. M. West and J. A. Dumesic, *Annu. Rev. Chem. Biomol. Eng.*, 2010, **1**, 79.

2 C. Zhao, T. Brück and J. A. Lercher, *Green Chem.*, 2013, **15**, 1720.

3 R. W. Gosselink, S. A. W. Hollak, S.-W. Chang, J. van Haveren, K. P. de Jong, J. H. Bitter and D. S. van Es, *ChemSusChem*, 2013, **6**, 1576.

4 B. Peng, Y. Yao, C. Zhao and J. A. Lercher, *Angew. Chem.*, 2012, **124**, 2114.

5 H. Zuo, Q. Liu, T. Wang, L. Ma, Q. Zhang and Q. Zhang, *Energy Fuels*, 2012, **26**, 3747.

6 M. Snåre, I. Kubičková, P. Mäki-Arvela, K. Eränen and D. Y. Murzin, *Ind. Eng. Chem. Res.*, 2006, **45**, 5708–5715.

7 J. Pérez-Ramírez, C. H. Christensen, K. Egeblad, C. H. Christensen and J. C. Groen, *Chem. Soc. Rev.*, 2008, **37**, 2530.

8 X. Zhang, D. Liu, D. Xu, S. Asahina, K. A. Cychosz, K. V. Agrawal, Y. Al Wahedi, A. Bhan, S. Al Hashimi, O. Terasaki, M. Thommes and M. Tsapatsis, *Science*, 2012, **336**, 1684.

9 C. Perego and A. Bosetti, *Microporous Mesoporous Mater.*, 2011, **144**, 28.

10 R. Nares, J. Ramírez, A. Gutiérrez-Alejandre, C. Louis and T. Klimova, *J. Phys. Chem. B*, 2002, **106**, 13287.

11 S. J. Gregg, *Adsorption Surface Area and Porosity*, 2nd edn, Academic Press Inc., New York, 1982.

12 J. Cejka, H. van Bekkum, A. Corma and F. Schueth, *Introduction to Zeolite Molecular Sieves*, 3rd edn, Elsevier Science, Amsterdam, 2007.

13 A. Corma, V. Fornes, L. Forni, F. Márquez, J. Martínez-Triguero and D. Moscotti, *J. Catal.*, 1998, **179**, 451.

14 M. M. J. Treacy and J. B. Higgins, *Collection of Simulated XRD Powder Patterns for Zeolites*, 5th Revised edn, Elsevier Science, Amsterdam, 2007.

15 B. Peng, C. Zhao, S. Kasakov, S. Foraita and J. A. Lercher, *Chem. – Eur. J.*, 2013, **15**, 4732.

16 B. Ma and C. Zhao, *Green Chem.*, 2015, **17**, 1692.

17 O. Y. Gutiérrez, Y. Yu, R. Kolvenbach, G. L. Haller and J. A. Lercher, *Catal. Sci. Technol.*, 2013, **3**, 2365.

18 A. de Mallmann and D. Barthomeuf, *J. Chim. Phys. Phys.-Chim. Biol.*, 1990, **87**, 535.

19 Z. Zhang, T. T. Wong and W. M. H. Sachtler, *J. Catal.*, 1991, **128**, 13.

20 T. J. McCarthy, G. D. Lei and W. M. H. Sachtler, *J. Catal.*, 1996, **159**, 90.

21 P. V. Menacherry and G. L. Haller, *J. Catal.*, 1998, **177**, 175.

22 L. Chen, J. Fu, L. Yang, Z. Chen, Z. Yuan and P. Lv, *ChemCatChem*, 2014, **6**, 3482.

23 H. Zuo, Q. Liu, T. Wang, L. Ma, Q. Zhang and Q. Zhang, *Energy Fuels*, 2012, **26**, 3747.

24 W. Song, Y. Liu, E. Baráth, C. Zhao and J. A. Lercher, *Green Chem.*, 2015, **17**, 1204.

25 A. Yu Stakheev and L. M. Kustov, *Appl. Catal., A*, 1999, **188**, 3.

26 W. M. H. Sachtler and A. Yu. Stakheev, *Catal. Today*, 1992, **12**, 283.